OPEN ACCESS Freely available online

PLOS ONE

I_h Tunes Theta/Gamma Oscillations and Cross-Frequency Coupling In an *In Silico* CA3 Model

Samuel A. Neymotin[1,2]*, Markus M. Hilscher[3,4], Thiago C. Moulin[5], Yosef Skolnick[1,6], Maciej T. Lazarewicz[7¤], William W. Lytton[1,8,9]

1 Department of Physiology & Pharmacology, State University of New York Downstate, Brooklyn, New York, United States of America, **2** Department of Neurobiology, Yale University School of Medicine, New Haven, Connecticut, United States of America, **3** Vienna University of Technology, Vienna, Austria, **4** Department of Neuroscience, Uppsala University, Uppsala, Sweden, **5** Medical Biochemistry Institute, Federal University of Rio de Janeiro, Rio de Janeiro, Brazil, **6** Computer Science Program, Brooklyn College, City University of New York, Brooklyn, New York, United States of America, **7** Department of Bioengineering, University of Pennsylvania, Philadelphia, Pennsylvania, United States of America, **8** Department of Neurology, State University of New York Downstate, Brooklyn, New York, United States of America, **9** Kings County Hospital, Brooklyn, New York, United States of America

Abstract

I_h channels are uniquely positioned to act as neuromodulatory control points for tuning hippocampal theta (4–12 Hz) and gamma (>25 Hz) oscillations, oscillations which are thought to have importance for organization of information flow. I_h contributes to neuronal membrane resonance and resting membrane potential, and is modulated by second messengers. We investigated I_h oscillatory control using a multiscale computer model of hippocampal CA3, where each cell class (pyramidal, basket, and oriens-lacunosum moleculare cells), contained type-appropriate isoforms of I_h. Our model demonstrated that modulation of pyramidal and basket I_h allows tuning theta and gamma oscillation frequency and amplitude. Pyramidal I_h also controlled cross-frequency coupling (CFC) and allowed shifting gamma generation towards particular phases of the theta cycle, effected via I_h 's ability to set pyramidal excitability. Our model predicts that *in vivo* neuromodulatory control of I_h allows flexibly controlling CFC and the timing of gamma discharges at particular theta phases.

Citation: Neymotin SA, Hilscher MM, Moulin TC, Skolnick Y, Lazarewicz MT, et al. (2013) I_h Tunes Theta/Gamma Oscillations and Cross-Frequency Coupling In an In Silico *CA3 Model. PLoS ONE* 8(10): e76285. doi:10.1371/journal.pone.0076285

Editor: Gennady Cymbalyuk, Georgia State University, United States of America

Received June 13, 2013; **Accepted** August 22, 2013; **Published** October 18, 2013

Funding: Research supported by National Institutes of Health grant R01MH086638 (http://nih.gov/). The funders had no role in study design, data collection and analysis, decision to publish, or preparation of the manuscript.

Competing Interests: The authors have no conflicts of interest to disclose. The authors would also like to state that WWL is a PLOS ONE Editorial Board member. This does not alter the authors' adherence to all the PLOS ONE policies on sharing data and materials.

* E-mail: samn@neurosim.downstate.edu

¤ Current address: Medtronic Neuromodulation, Minneapolis, Minnesota, United States of America

Introduction

The hyperpolarization-activated cyclic-nucleotide gated (HCN) channel is a voltage-gated ion channel involved in sub-threshold resonance [1–4]. Additionally, HCN plays an important role in regulating neuronal excitability by setting resting membrane potential (RMP) [5,6]. HCN produces the current known as I_h (*h* for hyperpolarization-activated), also known as I_f (*f* for funny), I_q (*q* for queer), and as "the anomalous rectifier". I_h is peculiar/funny/queer/anomalous because, unlike most channels, it inactivates with depolarization (hyperpolarization-activated). Another peculiarity is its mixed permeability, which gives it an intermediate reversal potential (E_{rev}) near −30 mV, unlike many channels which are dominated by a major permeability to Na^+, K^+, or Ca^{++}.

HCN channels are modulated by cyclic nucleotide second messengers. HCN has four isoforms which are differentially expressed in different cell types and differ in intrinsic properties, kinetics, and pharmacological sensitivities [1,7]. HCN1 and HCN2 isoforms are the dominant forms in hippocampus, and are present in varying proportions in all cell types studied. Of the two, HCN1 is faster (shorter time-constant).

In addition to its contribution to cell resonance, the HCN channel has a number of properties that suggest I_h might play a major role in control of oscillations in hippocampus and other brain areas: 1. It is one determinant of a critical cell-excitability control, RMP [5,8]. 2. It is differentially expressed in different cell types by virtue of inhomogeneous isoform distributions [1,3,7,9]. 3. It is differentially modulated in different cell types by virtue of targeting of particular excitatory or inhibitory cell types by particular neurotransmitters and neuromodulators projecting from different brain areas [2,10−13]. Because it is modulated through second messengers, these neurotransmitters and neuromodulators will be expected to have complex interactions within the cell chemistry prior to interacting with the membrane properties via I_h [14].

Hippocampus contains many classes of pyramidal and inhibitory cells, with differing contributions to network dynamics [15,16]. We hypothesized that differential modulation of I_h currents in different cell classes would fine-tune the power and frequencies of network-generated oscillations. We therefore investigated the effects of altering I_h conductance [14,17] in a computer model of hippocampal CA3, consisting of 800 pyramidal cells, 200 basket interneurons, and 200 oriens-lacunosum

moleculare cells [18], using different isoform combinations based on the literature [4,7,9]. We found that tuning I_h in different cell classes altered network rhythms, providing independent control for gamma and theta oscillations. I_h modulation also set the level of cross-frequency coupling and timing of gamma generation relative to the theta cycle. I_h modulation may therefore be an important control point with functional consequences, since these dynamics are hypothesized to contribute to learning and cognitive function [19–21].

Materials and Methods

Simulations

This model is an extension of a model of hippocampal CA3 that was previously published [18]. Simulations were performed on a Linux system with eight 2.27 GHz quad-core Intel Xeon CPUs using NEURON [22]. Eight seconds of simulation ran in about 2.2 minutes. In order to assess the robustness of the results, we ran each simulation condition with six different randomizations of synaptic inputs, and six different randomizations of network connectivity. Simulations were run in the NEURON simulation environment with python interpreter, multithreaded over 16–32 threads [22,23]. Analysis of simulation data was done with the Neural Query System [24] and Matlab (Mathworks, Inc.). The full model is available on ModelDB (https://senselab.med.yale.edu/modeldb).

Cells and connections

The network consisted of 800 five-compartment pyramidal (PYR) cells, 200 one-compartment basket (BAS) interneurons, and 200 one-compartment oriens lacunosum-moleculare (OLM) interneurons [25–27] (Fig. 1). Current injections (pyramidal cell s: 50 pA; OLM cells −25 pA) were added to get baseline activity. This was a simplification to substitute for absence of external inputs from other areas, and to compensate for the small size of the model, which did not allow for much self-activation.

All cells contained leak current, transient sodium current I_{Na}, and delayed rectifier current I_{K-DR}, to allow for action potential generation. Additionally, pyramidal cells contained in all compartments potassium type A current I_{K-A} for rapid inactivation, and hyperpolarization-activated current I_h based on HCN2 isoform parameterization [3,7]. Interneurons contained hyperpolarization-activated I_h current based on HCN1 isoform parameterization [3,7,9]. The OLM cells had a simple calcium-activated potassium current I_{KCa} to allow long lasting inactivation after bursting, high-threshold calcium current I_L to activate I_{KCa}, hyperpolarization-activated current I_h, and intracellular calcium concentration dynamics. Selection of currents was based on prior published models [25,28–30] and basket interneuron I_h currents were based on the literature [3,7,9].

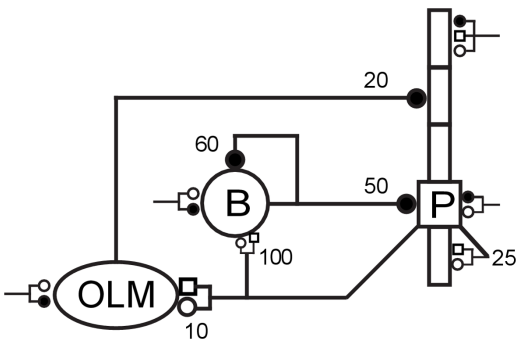

Figure 1. Schematic representation of the network. Each symbol represents a population: 800 pyramidal cells (P), 200 basket cells (B), 200 OLM cells. Convergence values (number of inputs for an individual synapse) are shown near synapses: $GABA_A$ receptors (filled circles), AMPA receptors (open circles), NMDA receptors (open squares). External stimulation from other areas was modeled by synaptic bombardment (synapses with truncated lines).
doi:10.1371/journal.pone.0076285.g001

For all cell types the I_h current was defined as $I_h = g \cdot (v - e_h)$, where g is the instantaneous conductance, v is the membrane potential, and e_h is the reversal potential (−30 mV for BAS and PYR cells; −40 mV for OLM cells). Each I_h channel had a parameter, $\bar{g}$, which represented the maximal conductance density (0.0002 S/cm^2 for BAS, 0.0001 S/cm^2 for PYR, and 0.00015 S/cm^2 for OLM cells). To simulate neuromodulatory scaling of the I_h conductance values, $\bar{g}$ was multiplied by another factor, f, which varied between 0.0 and 2.0, and was set to 1.0 for the baseline simulations. Instantaneous conductance was then set to $\bar{g} \cdot h \cdot f$, where h is the I_h gating variable which activated at hyperpolarized voltages. The evolution of the h state variable in time followed $\dot{h} = (h_\infty - h)/\tau_h$, where h_∞ was the voltage-dependent steady-state value of h, and τ_h was the voltage-dependent time-constant of h (in milliseconds).

For BAS cells, h_∞ was set to $1/(1+e^{0.151 \cdot (v - v_{50})})$, where v was the membrance voltage, and v_{50}, the $\frac{1}{2}$-maximal voltage level, was set to −73 mV. BAS cell τ_h followed $e^{0.033 \cdot (v+75)}/(0.011 \cdot (1+e^{0.083 \cdot (v+75)}))$. PYR h_∞ followed $1/(1+e^{(v - v_{50})/10.5})$, with v_{50} at −82 mV. PYR τ_h was set to $1/(e^{-14.59 - 0.086 \cdot v} + e^{-1.87 + 0.0701 \cdot v})$. OLM h_∞ followed $1/(e^{((v+80)/10)} + 1)$, and OLM τ_h followed $200/(e^{(v+70)/20} + e^{-(v+70)/20}) + 5$.

I_h-static. To test the effect that I_h had on individual neurons, we isolated the dynamic component, which had the voltage-dependent conductance (g) described above. To do this, we first ran a set of 7 second simulations, varying the f parameter from 0.0 to 2.0 (with increments of 0.5) and measured the I_h conductance (g) at the end of each simulation. This conductance (g) was saved for each compartment of each cell type. I_h-static was then defined as the current from a leak channel with conductance equal to g measured in the previous step, and with the same reversal potential (e) as the original I_h channel. I_h-static followed $i = g \cdot (v - e)$.

The network contained 152,000 synapses. Pyramidal cell projections were mixed alpha-amino-3-hydroxy-5-methyl-4-isoxazolepropionic acid (AMPA) and N-methyl-D-aspartic acid (NMDA) response. Basket cells synapsed on the soma of both pyramidal cells and other basket cells via gamma-aminobutyric acid A ($GABA_A$) receptors. OLM cells connected to distal dendrites of pyramidal cells via $GABA_A$ receptors. AMPA and NMDA receptors had reversal potentials of 0 mV, while $GABA_A$ receptors had reversal potentials of −80 mV.

Connections in the network were set up based on fixed convergences (Table 1). However, connectivity was random and specific divergence could therefore vary. All synaptic delays between cells were 2 ms, to simulate axonal propagation and neurotransmitter diffusion and binding, which were not explicitly modeled. Parameters were based on the literature where available, as well as on previous models [25,31].

Synapses

Synapses were modeled by a standard NEURON double-exponential mechanism with parameters based on Tort *et al.*, 2007 [25] (Table 1). Magnesium block in NMDA receptors used the

Table 1. Synaptic parameters.

Presynaptic	Postsynaptic				Receptor	τ_1 (ms)
τ_2 (ms)					Conductance (nS)	Convergence
Pyramidal	Pyramidal	AMPA	0.05	5.3	0.02	25
Pyramidal	Pyramidal	NMDA	15	150	0.004	25
Pyramidal	Basket	AMPA	0.05	5.3	0.36	100
Pyramidal	Basket	NMDA	15	150	1.38	100
Pyramidal	OLM	AMPA	0.05	5.3	0.36	10
Pyramidal	OLM	NMDA	15	150	0.7	10
Basket	Pyramidal	$GABA_A$	0.07	9.1	0.72	50
Basket	Basket	$GABA_A$	0.07	9.1	4.5	60
OLM	Pyramidal	$GABA_A$	0.2	20	72	20

doi:10.1371/journal.pone.0076285.t001

experimental scaling factor $1/(1+0.28\cdot Mg\cdot e^{-0.062\cdot V})$; $Mg = 1mM$ [32].

Background activity

Throughout the simulation duration, background activity was simulated by synaptic excitatory and inhibitory inputs following a Poisson process, sent to somata of all cells and dendrites of pyramidal cell s (Table 2). Fast background activity consisted of AMPA and GABA-ergic bombardment at 1000 Hz. Slow activity used activation of the NMDA receptors at a mean frequency of 10 Hz. These inputs represented the influence of surrounding excitatory and inhibitory cells not explicitly modeled in the simulation and produced a high conductance state similar to that observed *in vivo* [33]. In addition, we placed slow excitatory inputs in the last distal apical compartment of pyramidal cells, in order to model input from the entorhinal cortex. This input was capable of simulating calcium-spike-like activity in the dendritic compartment and driving sparse firing of pyramidal cells. Synapses were activated randomly according to a Poisson distribution.

Local field potential (LFP) was simulated by a sum of differences in membrane potential between the most distal apical and the basal dendritic compartment over all pyramidal cells. Before calculating spectral power, the DC component of the signal was removed [34]. In addition, the first and last 200 ms of simulated data were removed to avoid artifacts associated with endpoints in the data. The spectral power was calculated using the multitaper method (MatLab pmtm() function; Mathworks, Inc.). Peak values in the power spectra are reported for theta ($4-12$ Hz) and low gamma ($25-55$ Hz) frequency bands. All *r*-values reported were calculated using the Pearson correlation coefficient. To determine cross-frequency-coupling (CFC) between theta and gamma oscillations, we used a modified version of the modulation index [35] to reduce artifacts in CFC measures associated with sharp spikes [36]. Theta oscillations were extracted by filtering LFPs between 6–10 Hz using a zero phase distortion band-pass filter. Gamma spikes (duty cycle between 18–40 ms, corresponding to 55–25 Hz) were extracted using a time-domain feature-extraction method [37]. Theta phases at times of gamma spike peaks were then used to form the gamma-amplitude/theta-phase measure, which consisted of 100 equally-spaced phase bins, and were then used to calculate the modulation index [35].

Table 2. Parameters for modeling background activity.

Cell	Section	Synapse	τ_1 (ms)	τ_2 (ms)	Conductance (nS)
Pyramidal	Soma	AMPA	0.05	5.3	0.05
Pyramidal	Soma	$GABA_A$	0.07	9.1	0.012
Pyramidal	Dend	AMPA	0.05	5.3	0.05
Pyramidal	Dend	NMDA	15	150	6.5
Pyramidal	Dend	$GABA_A$	0.07	9.1	0.012
Basket	Soma	AMPA	0.05	5.3	0.02
Basket	Soma	$GABA_A$	0.07	9.1	0.2
OLM	Soma	AMPA	0.05	5.3	0.0625
OLM	Soma	$GABA_A$	0.07	9.1	0.2

doi:10.1371/journal.pone.0076285.t002

Final evaluations to produce the results presented here were made over the course of 1044 network simulations, using six different random wirings, six different input streams, and variations in maximal I_h conductance level (relative to baseline: 0.0, 0.5, 1.0, 1.5, 2.0) at the different cell types, where baseline is the I_h density estimated from the literature. A typical network simulation (8 s; 1200 neurons) took approximately 2.2 minutes using 16 threads on a 2.27 GHz Intel Xeon quad core CPU.

A long-duration simulation set (900 seconds for each simulation) was run using 5 I_h levels for the pyramidal and basket cells. These simulations all had identical wiring and input streams. The data obtained were used to evaluate theta/gamma cross-frequency-coupling and phase relationships as a function of I_h level.

An additional set of simulations of isolated cells was run, varying I_h conductance level in the same amounts as in the network. These simulations were used to assess I_h effects on resting membrane potential (RMP) and synaptic integration. These simulations were run for 7 s to allow the cells to reach a steady-state where net transmembrane currents were zero. Then, I_h conductance was measured and was used to set a fixed conductance with equivalent E_{rev} to I_h, to separate I_h dynamics from its static features. In these simulations, AMPA and $GABA_A$ inputs (0.5 nS) were provided at 5.5 s to assess post-synaptic-potential amplitude and temporal integration.

Results

This study involved over 1000 eight-second network simulations, testing six different input streams, and variations in maximal I_h conductance level for the different cell types. These are presented as $0.0\times I_h$, $0.5\times I_h$, $1.0\times I_h$, $1.5\times I_h$, $2.0\times I_h$, relative to a baseline set to a standard I_h density estimated from the literature. In order to ensure robustness of the results shown, each simulation was tested with six different wirings (wiring density is parameterized but specific point-to-point wiring is random). An additional set of 25 long-term (900 second) simulations were run to evaluate theta/gamma cross-frequency-coupling and phase relationships as a function of I_h level. Simulations were run using the NEURON simulator on Linux on a 2.27 GHz quad-core Intel XEON CPU. Eight seconds of network simulation ran in $\sim$2.2 minutes.

I_h is a prominent part of resting conductance, contributing to resting membrane potential (RMP), due to the presence of non-zero I_h conductance at RMP, and to a relatively depolarized reversal potential (E_{rev}). The isolated model oriens-lacunosum moleculare (OLM) cell was depolarized with increasing I_h, from

−68.1 mV without I_h, to −64.3 mV at 0.5×, to −61.8 mV at $1 \times I_h$. Increasing I_h past baseline produced further depolarization and cell firing. At $1.5 \times I_h$, the OLM produced a single action potential and then stabilized with an RMP of −59.5 mV. Further increase to $2 \times I_h$ produced rhythmic firing at 6 Hz, a low theta frequency. Pyramidal (PYR) and basket (BAS) cells displayed monotonic RMP dependence on I_h, with RMP ranging from −65.6 – −57.5 mV and −65 – −61.7 mV, respectively. PYR cells emitted one and two transient spikes at 1.5 and $2 \times I_h$, respectively, while BAS cells did not exhibit any spontaneous firing.

Altering I_h altered both the magnitude and time-course of excitatory and inhibitory postsynaptic potentials (EPSPs and IPSPs). Both types of PSP showed increasing amplitude with increasing I_h. IPSP amplitude increase can be directly explained as a consequence of the greater driving force at the more depolarized RMP. With $0-2 \times I_h$, BAS and PYR increases were from 0.30–0.44 mV and 0.49–1.1 mV, respectively, while OLM increased from 0.22–0.65 mV, with $0-1.5 \times I_h$ (at $2 \times I_h$, OLM fired rhythmically, precluding accurate IPSP measurement).

EPSP amplitude was also generally augmented with I_h increase (Fig. 2a). This is a paradoxical effect, given that the direct RMP depolarizing shift that augmented IPSP driving force decreased EPSP driving force. In addition to reducing driving force, increased I_h also increased shunting, an effect that would reduce amplitude of both EPSPs and IPSPs. Both of these static factors predict EPSP amplitude *decrease*. We therefore predicted that replacement of the dynamical I_h with a static version (fixed conductances of equivalent magnitudes and E_{rev}; see Materials and Methods) would reduce EPSP amplitude. Instead, we found even larger increases in EPSP magnitude. Examination of transmembrane current activations of both Na^+ and K^+ currents, revealed a larger depolarizing effect of I_{Na} (Fig. 2b), which dominated over the hyperpolarizing effect of I_K (Fig. 2c). With block of Na^+ and K^+ channels, EPSP amplitudes decreased with depolarized RMP, as originally predicted. The dynamics of I_h itself worked to reduce this amplitude increase: I_h turns off during the EPSP, reducing the degree of depolarization and reducing the I_{Na} boost (Fig. 2d). The combination of these 5 effects (driving force,shunting, I_{Na}, I_K, I_h dynamics) produced a mild overall EPSP amplitude increase, that was far less pronounced than the increase in IPSP: BAS: 0.99–1.17 mV with $0-2 \times I_h$; PYR 1.78–2.21 mV with $0-1.5 \times I_h$, $2 \times I_h$ produced spiking; OLM 0.96–1.07 mV, with $0-1 \times I_h$, $1.5 \times I_h$ produced spiking. In one case, a slight decrease in EPSP amplitude was seen: 1.78 to 1.72 mV with increase of I_h from 0 to 0.5× baseline in the PYR cell.

Time to peak PSP was delayed by increasing I_h. These effects were again a result of multiple conflicting tendencies. We therefore looked separately at the effects of the conductance change, effects of other channels, and effects of I_h dynamics themselves. The conductance change alone lowered R_{in} which reduced membrane time-constant, which reduced the duration of synaptic response, leading to an earlier peak. Returning Na^+ and K^+ currents to the simulation moved PSP peaks to slightly later times. Adding back the dynamics of I_h moved the PSPs to earlier times again. With all these dynamical factors in place, IPSP delays had noticeably increasing values: BAS 10.8–12.5 ms with $0-2 \times I_h$; PYR 6.8–9.5 ms with $0-2 \times I_h$; OLM 10.0–16.5 ms with $0-1.5 \times I_h$ since $2 \times I_h$ produced rhythmic spiking. Similar effects were observed for EPSP delays (BAS: 8.6–10.7 ms with $0-2 \times I_h$; PYR: 4.9–8.1 ms with $0-1.5 \times I_h$ since at $2 \times I_h$ the synaptic input produced a spike; OLM: 7.6–9.5 ms with $0-1.5 \times I_h$).

In the network, baseline firing rates of PYR, BAS, and OLM cells were 1.8 Hz, 10.8 Hz, and 1.2 Hz, respectively. As a population, OLM cells tended to fire rhythmically at theta frequency (4−12 Hz). Interactions between cells in the network led to the generation of theta and gamma (>25 Hz) oscillations (Fig. 3). These emergent rhythms were generated through the different synaptic time constants in the network and through the cellular interactions of pyramidal-interneuron network gamma (PING) and interneuron network gamma (ING) [15,31,38,39].

Baseline oscillations were similar to those described in earlier versions of this model, which contained I_h currents in PYR but not in BAS cells [18]. Briefly, strong periodic OLM firing shut down PYR activity resulting in lower PYR → BAS drive. PING interactions between PYR and BAS cells contributed to gamma oscillations: lower PYR to BAS drive led to lower gamma amplitude during periods of OLM → PYR inhibition. As the PYR cells recovered from OLM inhibition, their activity gradually built up providing increased drive to BAS cells and increasing gamma amplitudes, accounting for nesting of gamma within the theta cycle (Fig. 3a,b). ING also contributed to the strength of gamma in this model due to strong BAS → BAS connectivity. The presence of I_h led to a slightly higher gamma amplitude than in the prior model due to the stronger repolarization enhancing the ING mechanism. Individual cell voltages showed multiple rhythms as well, with both the PYR and BAS cells reflecting the network oscillation in their postsynaptic potentials (Fig. 3c).

Given the complex of RMP shifts and temporal integration properties through PSP alterations in the individual cells, we hypothesized that I_h changes would substantially alter frequency and power in network rhythms. Testing I_h modulation across different cell types within the full network demonstrated consistent but dramatically different effects depending on which cell type was targeted. We started by looking at OLM cells because they provide a central modulating role for theta activity (Fig. 4, Fig. 5) [18]. Reducing or eliminating I_h from OLM cells abolished theta by eliminating the depolarizing influence of I_h. The resulting hyperpolarization reduced OLM firing rate (1.2−0.2 Hz) which reduced theta modulation throughout the network (red and black in Fig. 4a,b; Fig. 5a,b). The reduced inhibition coming from OLM cells resulted in higher firing rates of PYR cells (1.8−3.5 Hz), which then strengthened BAS activity (10.8−28.7 Hz). The increased dominance of PYR and BAS populations produced a large increase in gamma power (inset in Fig. 4b right) created via the PING mechanism. Increasing OLM I_h conductance from baseline increased OLM firing rate (1.2−2.8 Hz) and caused the OLM inhibition of the network to dominate, gradually reducing both theta and gamma power as PYR and BAS rates went towards zero (PYR:1.8−0.4 Hz; BAS:10.8−2.0 Hz; Fig. 5e).

Increasing I_h conductance across all cellular locations produced effects primarily similar to the effects on OLM, with reduced theta power and augmented gamma at reduced I_h amplitudes. These effects were brought about via the strong governing inhibitory influence of OLM cells, which increased at heightened I_h levels. As with OLM I_h enhancement, higher I_h values showed decrease in gamma power and frequency with increase in theta.

BAS cells are particularly involved in both ING (BAS-BAS) and PING (PYR-BAS) mechanisms of gamma generation [38,39]. Hence, it was not surprising that variation of BAS I_h altered gamma power and frequency consistently with no consistent effect on theta (Fig. 6, Fig. 7). Increased BAS I_h augmented gamma power ($r=0.88; p<1e-9; n=180$) and reduced gamma frequency ($r=-0.56; p<1e-9; n=180$). The increased power corresponded to increase in the BAS population firing rates (9.1−12.6 Hz with I_h $0-2\times$) due to the depolarizing effect of I_h. These increases in BAS firing also dampened PYR firing (1.8−1.7 Hz), which secondarily reduced OLM activity (1.3−1.2 Hz). The decreased gamma frequency was due to the

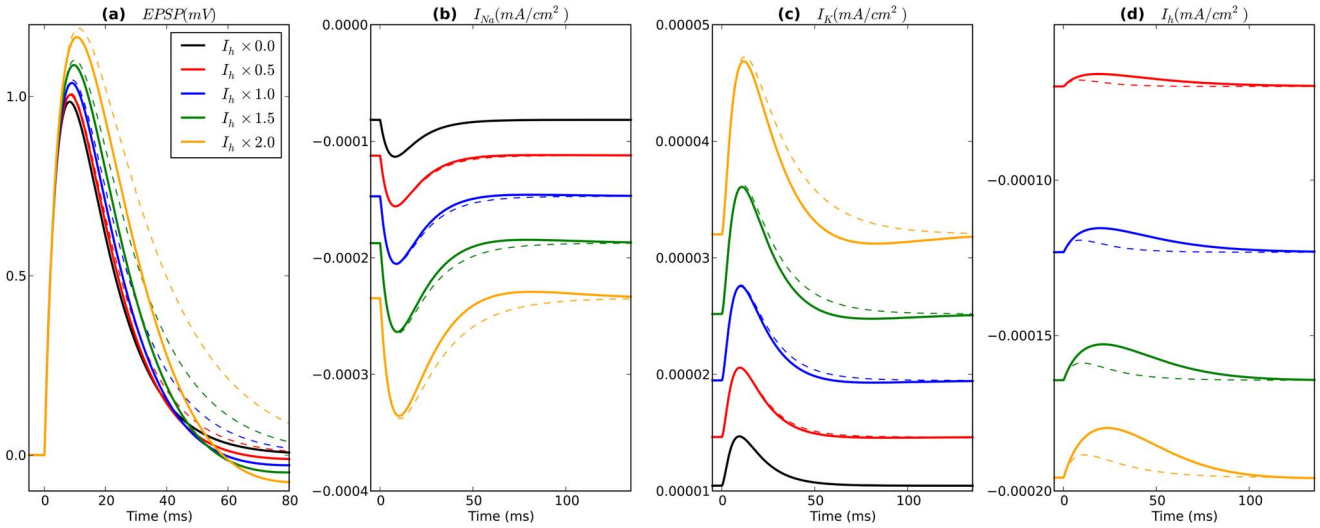

Figure 2. BAS cell response to AMPA stimulus at different levels of I_h conductance. Solid lines represent responses with dynamic I_h and dotted lines represent responses with static I_h. Note that only BAS cell is displayed since it did not fire action potentials in response to AMPA-ergic stimulation. Time axes are relative to AMPA input at $t=0$ ms. (**a**) EPSP (starting voltage levels aligned vertically for easier comparison of EPSPs), (**b**) I_{Na}, (**c**) I_K, and (**d**) I_h at BAS cell soma.
doi:10.1371/journal.pone.0076285.g002

longer synaptic integration times that the BAS cells displayed with enhanced I_h.

By contrast with BAS I_h effects, PYR I_h effect was primarily on theta, progressively increasing theta peak ($r=0.89; p<1e-9; n=180$) and power ($r=0.73; p<1e-9; n=180$; Fig. 8, Fig. 9; consistent with experiment [40]). Increases in theta peak and power were effected through increased PYR firing (1.6–1.9 Hz) which produced increased OLM firing (0.9–1.6 Hz). Unlike in Fig. 4, OLM firing did not suppress PYR firing since PYR activity was the driving force and was supported by the PYR I_h. Due to PING interplay, gamma oscillation power was positively correlated with PYR I_h level ($r=0.73; p<1e-9; n=180$; BAS rates: 9.2–12.1 Hz). Although gamma peak frequency was not significantly shifted, there was some broadening with increasing PYR I_h. Overall PYR I_h modulation tuned both theta and gamma power together, distinct from other pharmacological effects where theta and gamma are inversely correlated [18].

The contrast of a nearly orthogonal arrangement of strong influence of PYR I_h on theta and strong influence of BAS I_h on gamma led us to hypothesize that detailed control of network oscillation could be effected through comodulation of I_h in both. This comodulation could involve simultaneous control where I_h in both cell types were altered together. Alternatively, more complex modulation could occur via activation through different second messengers, or different isoform second-messenger sensitivity, through activation by a neuromodulator with divergent downstream effects. Simultaneous I_h modulation of both PYR and BAS cells produced an additive effect, with changes in both theta and gamma rhythms (Fig. 10, Fig. 11). There was a clear trend of progressively increasing theta peak ($r=0.91; p<1e-9; n=180$) and a similar trend for increasing theta power ($r=0.72; p<1e-9; n=180$). The changes in theta power were brought about by increased PYR firing (1.6–1.9 Hz) which drove increases in OLM firing (0.9–1.6 Hz). Similar to the simulations where PYR I_h was modulated independently, OLM firing did not suppress PYR firing due to I_h increases supporting PYR activity. Gamma oscillation power had a large positive correlation with PYR and BAS I_h levels ($r=0.93; p<1e-9; n=180$) due to direct enhancement to BAS population activity via I_h (8.0–14.1 Hz) and also secondarily due to PING mechanisms. Gamma peak frequency had a clear trend of reduction with increases in PYR and BAS I_h ($r=-0.69; p<1e-9; n=180$), due to the extended delays to peak IPSPs and EPSPs that PYR and BAS cells exhibited with increasing I_h.

HCN1 and HCN2 have different molecular modulators: cAMP selectively modulates HCN2, [41,42] while p38 MAP kinase modulates HCN1 [43]. However, the complexity of linkages from neuromodulators to expression of second and third messengers, and the consequent control in HCN isoforms by these messengers, is currently inaccessible to simulation. We therefore assessed all combinations of I_h modulation at PYR and BAS cells in order to observe the patterns of gamma-theta relations that could be expressed through HCN modulation in this system. As expected from the relative independence of gamma and theta control from the cell types, we found that these patterns were highly constrained (Fig. 12). Both theta amplitude and frequency increased with PYR I_h level with effectively no effect of BAS I_h levels (Fig. 12a,b).

Although gamma frequency (Fig. 12c) and amplitude (Fig. 12d) showed primary control by BAS I_h as expected, there was also a prominent effect of PYR I_h, producing the greatest overall gamma amplitude augmentation with coordinated increase in both BAS and PYR I_h. Hence the highest gamma amplitude and highest gamma frequency also showed correlation with the highest theta amplitude and frequency.

Cross-frequency-coupling (CFC) measures the ability of the slower theta wave to provide an envelope that modulates the amplitude of the superimposed faster gamma. Since the strong OLM inhibition only allowed co-expression of theta and gamma oscillations in a relatively narrow range of OLM I_h, we only measured CFC as a function of PYR and BAS I_h. Substantial CFC was only present with high PYR I_h, corresponding to large theta (Fig. 12e). The difference between low and high CFC can be seen in Fig. 10a. The black trace demonstrates low CFC: at left only a little alteration of gamma amplitude with theta is seen; at right there is almost no gamma hence no coupling. By

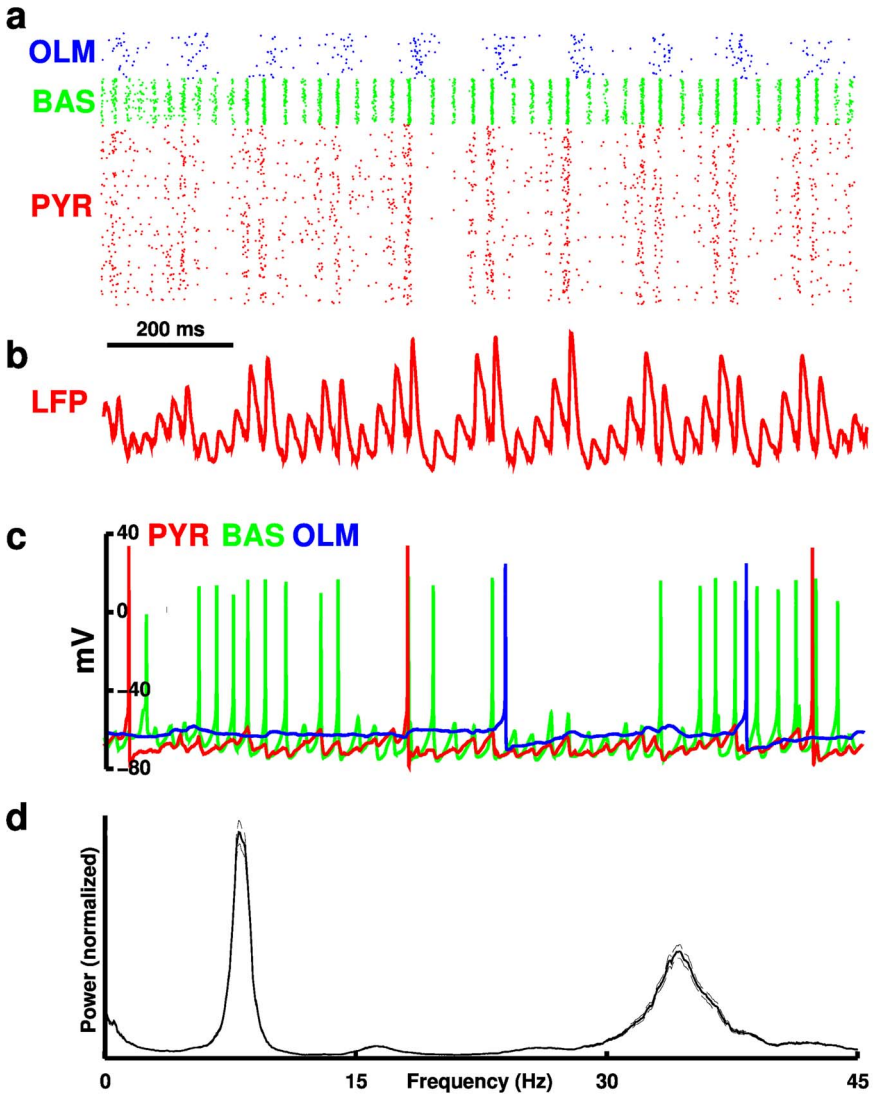

Figure 3. Activity of network at baseline. (**a**) Raster plot showing firing times of cells within the network. Cell types are color-coded. (**b**) Local field potential (LFP) generated by PYR cells. (**c**) Voltage traces from soma of different cell types. (**d**) Average ($n=36$) local field potential power spectrum $\pm$ standard error of the mean (SEM; dotted lines).
doi:10.1371/journal.pone.0076285.g003

contrast the orange trace shows substantial coupling, most readily seen in the 4th theta cycle. Note that these cycle-to-cycle differences make the overall CFC difficult to calculate. In this high PYR I_h regime, coupling was highest at low values of BAS I_h, where average gamma activity, reflecting this modulation from low to high, was low (Fig. 12d). By contrast high BAS I_h corresponded to a strong continuous gamma which was not as readily modulated. Peak coupling corresponded to oscillations with gamma frequency of 33.5 Hz and theta frequency of 8.6 Hz.

Across I_h levels, the peak gamma amplitude always occurred during the positive portion of the theta cycle (Fig. 12f), slightly after the theta peak from $\frac{\pi}{6}$ to $\frac{\pi}{4}$ radians ($\sim$0.5–0.8, where 0 is theta peak). This is consistent with experimental data, which shows peak amplitude of gamma occurring on the positive but descending portion of the theta oscillation [44]. Increased PYR I_h shifted peak gamma amplitude towards earlier phases of the theta cycle. This was due to the depolarizing effects of PYR I_h producing heightened PYR excitability, leading to earlier PYR cell firing, and hence earlier production of gamma via PING. Reduced phase lag was therefore associated with stronger CFC ($r=-0.81; p<1e-5; n=25$).

At baseline, PYR spiking tended to occur near the peak of theta ($\pm\frac{\pi}{16}$ radians), earlier than the theta phase for maximum gamma. This delay from peak PYR firing to peak local field gamma is consistent with a PING mechanism: peak PYR firing engages a larger number of inhibitory cells. This then leads to a subsequent peak gamma cycle, representing the maximum proximal/distal synaptic-activation differences, which then occurs on the subsequent cycle.

Discussion

Our modeling predicts that neuromodulation of I_h conductance could have several functional roles in *in vivo* neuronal dynamics including: 1) tuning of theta and gamma oscillation amplitude and frequency, 2) modulation of cross-frequency coupling (CFC) levels, and 3) enhanced excitability of cells within a circuit, expressed as

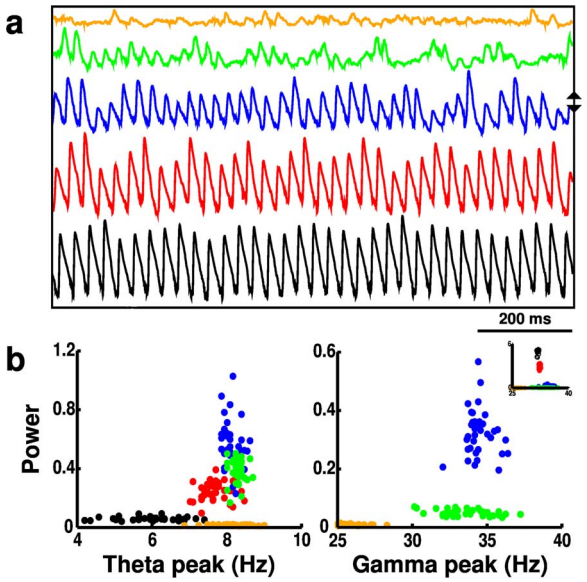

Figure 4. Activity (from 180 simulations) with I_h scaling in OLM interneurons. (**a**) Local field potentials (LFPs). Blue LFP is from baseline simulation. Up (down) arrows indicate directions of increase (decrease) of I_h. (**b**) Scatter plots of theta (left) and gamma (right) peak frequencies and power (normalized); color code as in (**a**); each point from a single simulation with different random activation and wiring. Gamma: main panel shows zoom-in of subset of values. Inset shows full set.
doi:10.1371/journal.pone.0076285.g004

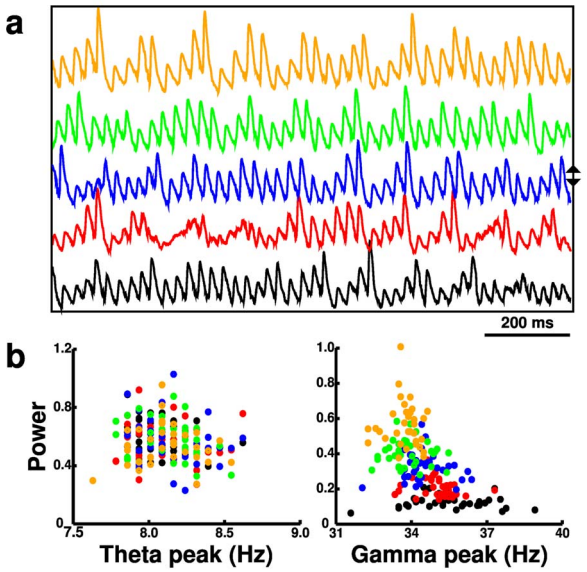

Figure 6. Activity (from 180 simulations) with I_h scaling in basket (BAS) interneurons. (**a**) Local field potentials (LFPs). Blue LFP is from baseline simulation. Up (down) arrows indicate directions of increase (decrease) of I_h. (**b**) Scatter plots of theta and gamma peak frequencies and power (normalized).
doi:10.1371/journal.pone.0076285.g006

increased gamma oscillation amplitude at earlier phases of the theta cycle. I_h is uniquely positioned for these roles for several reasons: 1) I_h enhances resonance in individual neurons, 2) I_h contributes to resting membrane potential, and hence neuronal excitability, 3) multiple HCN isoforms are differentially expressed in different cell types known to contribute to different oscillation frequencies, and 4) neuromodulators allow precise control of the conductance of specific HCN isoforms via second-messenger signaling cascades [7,43]. These functions of theta and gamma oscillations are linked to different aspects of cognition and behavior: CFC level is correlated with hippocampal-dependent learning performance [21,45] and attentional modulation [46],

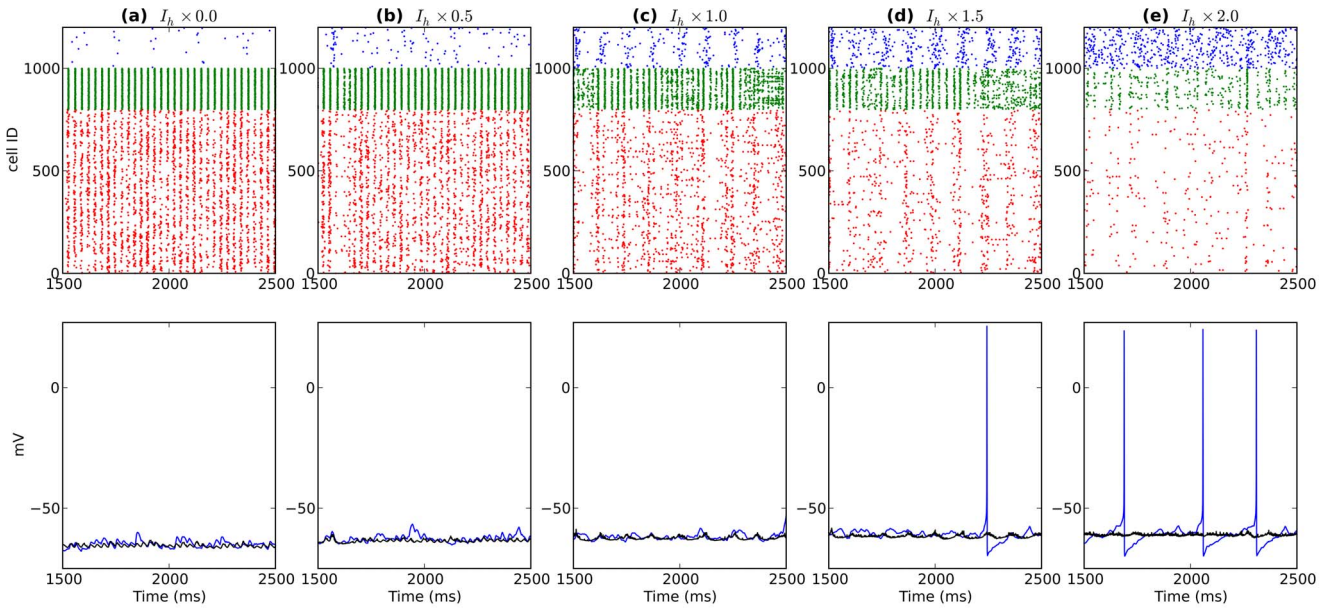

Figure 5. Activity from a single network after modulating OLM I_h levels (OLM I_h increases left to right). Top shows spike rasters (PYR:red; BAS:green; OLM:blue). Bottom displays somatic voltage from a single OLM cell (blue) and average somatic voltage from 200 OLM cells (black).
doi:10.1371/journal.pone.0076285.g005

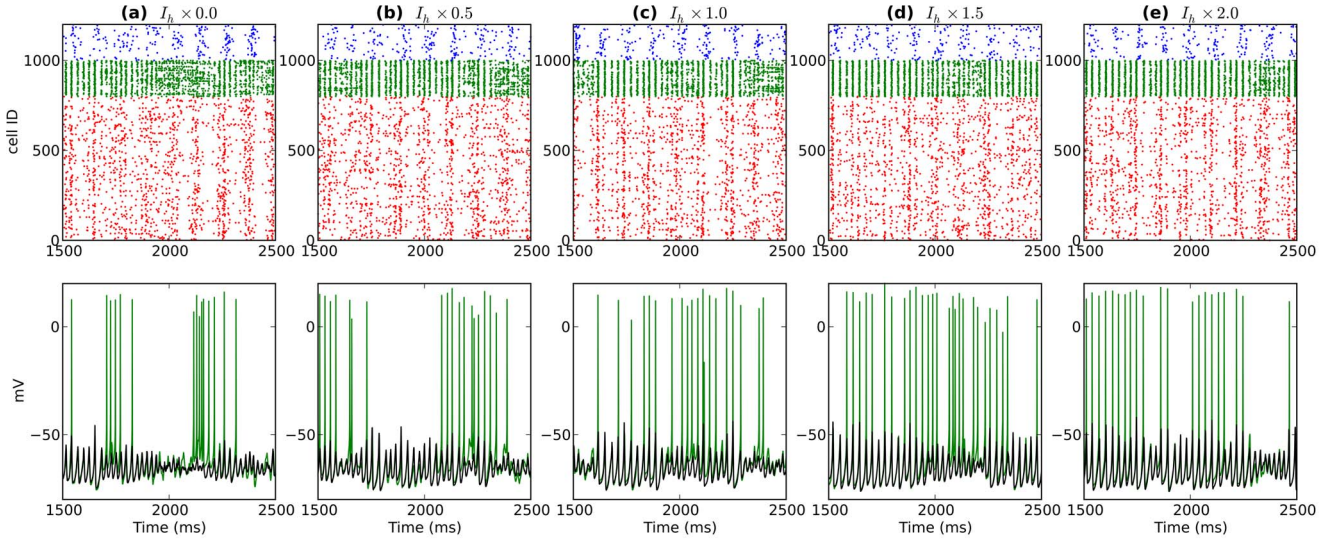

Figure 7. Activity from a single network after modulating BAS I_h levels (BAS I_h increases left to right). Top shows spike rasters (PYR:red; BAS:green; OLM:blue). Bottom displays somatic voltage from a single BAS cell (green) and average somatic voltage from 200 BAS cells (black).
doi:10.1371/journal.pone.0076285.g007

and gamma nesting within theta oscillations is a hypothesized mechanism for encoding information dynamically [20].

We investigated I_h channel function in a multiscale model across levels from ion channel population to the neuronal network. Emergent predictions arose at the levels of channel interactions in dendrites, of dendritic signal interactions in cells and of neurons forming the network. At the dendritic and cellular level, I_h generally increased both EPSP and IPSP magnitude and duration with some variation by cell type. At the cell level, excitability increased due to cell depolarization. At the network level, I_h modulation altered both theta and gamma, with effects depending on where in the circuit the modulation occurred. As we have previously shown, OLM provides control over theta activation in the network due to its long time constants [18]. Reduced OLM I_h eliminated theta by removing this influence (Fig. 4, Fig. 5). This then allowed the PYR and BAS interactions to create strong, continuous gamma through ING and PING mechanisms. Increased OLM I_h eliminated all activity by causing increased OLM activity which shut down activity in the other cells, OLM being an inhibitory cell type. Modulating I_h across all cell types had effects similar to those seen with OLM modulation, due to this strong governing influence of OLM.

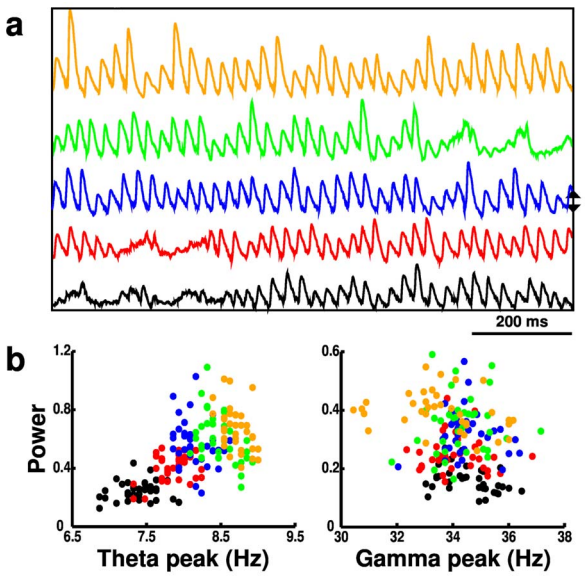

Figure 8. Activity (from 180 simulations) with I_h scaling in pyramidal (PYR) cells. (**a**) Local field potentials (LFPs). Blue LFP is from baseline simulation. Up (down) arrows indicate directions of increase (decrease) of I_h. (**b**) Scatter plots of theta and gamma peak frequencies and power (normalized).
doi:10.1371/journal.pone.0076285.g008

Different neurotransmitters are likely to have differential effects on different cell types through effects on different receptors on the different cell types. Our modeling suggests likely cellular locations of neuromodulation targets for changing oscillation power and frequency. These could be tested by using immunohistochemistry to correlate the location of neurotransmitter receptor types with particular cell types. For example, it is known that noradrenaline is involved in I_h regulation [47]. In addition, recent experimental evidence demonstrates that acetylcholine modulates different features of I_h activity, including its sag amplitude [11,12]. Interestingly, acetylcholine has also been shown to contribute to modulation of theta frequency over a range similar to that observed in our model [48].

The BAS cell is particularly involved in the genesis of gamma oscillations through the ING (BAS-BAS) and PING (PYR-BAS) mechanisms. Increased BAS cell I_h increased BAS activity and raised gamma power (Fig. 6, Fig. 7). This increase also slightly lowered gamma frequency, due to the increased duration of synaptic responses. The PYR cell is the only excitatory cell in the network and therefore plays a role in maintaining firing of all cell types. Increased PYR I_h increased PYR → OLM activation and produced a monotonically increasing effect on both power and frequency of theta (Fig. 8, Fig. 9). Note that this apparent PYR → OLM effect was quite different than the more direct activation provided by increasing OLM I_h. At the same time, the increased PYR → BAS activation produced a tendency to increased gamma power without consistent effect on frequency. The overall PYR effect was to tune both theta and gamma power together, distinct

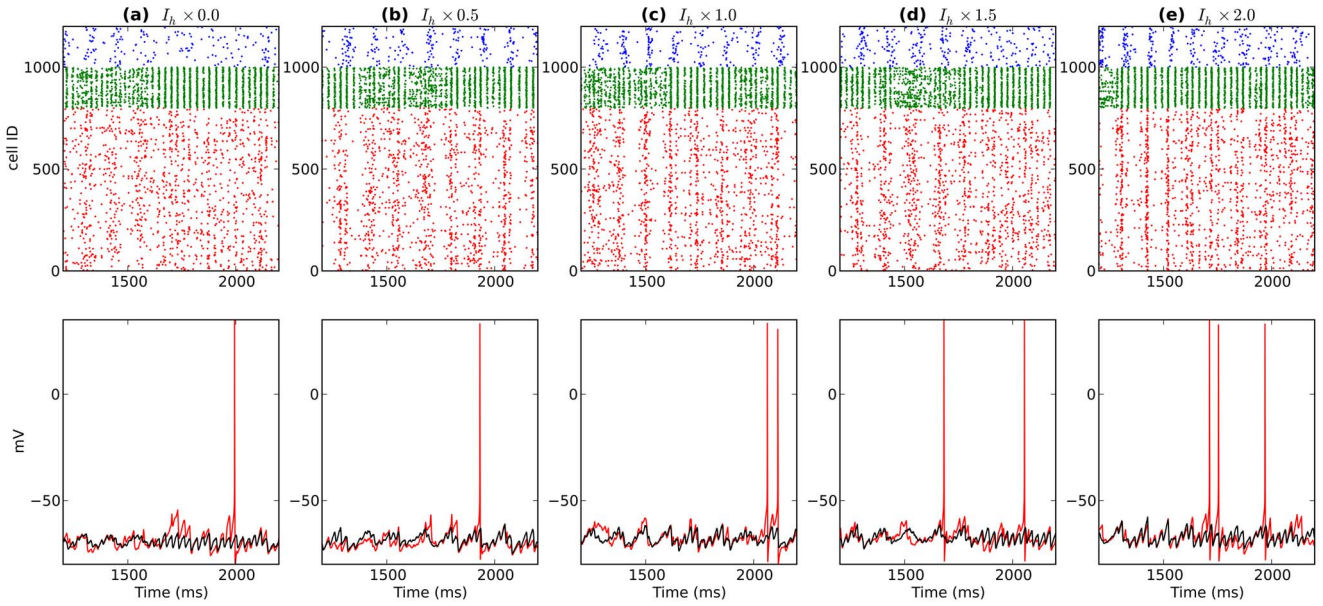

Figure 9. Activity from a single network after modulating PYR I_h levels (PYR I_h increases left to right). Top shows spike rasters (PYR:red; BAS:green; OLM:blue). Bottom displays somatic voltage from a single PYR cell (red) and average somatic voltage from 800 PYR cells (black).
doi:10.1371/journal.pone.0076285.g009

from other pharmacological effects where theta and gamma trade off [18].

Simultaneous modulation of PYR and BAS I_h similarly comodulated power, while now shifting both frequencies consistently: gamma tuning towards lower frequency while theta tuned towards higher frequency with increased I_h (Fig. 10, Fig. 11). Independent modulation of PYR and BAS I_h allowed flexible control of the frequencies and amplitudes of theta and gamma oscillations (Fig. 12a,b,c,d). We hypothesized that these

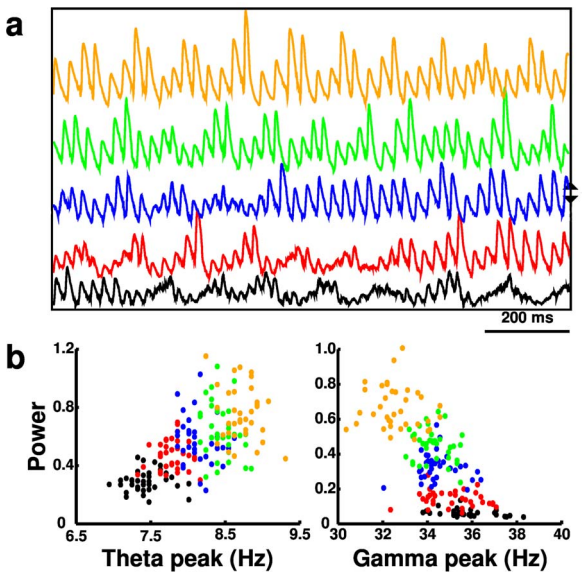

Figure 10. Activity (from 180 simulations) with I_h scaling in both pyramidal (PYR) and basket (BAS) cells. (**a**) Local field potentials (LFPs). Blue LFP is from baseline simulation. Up (down) arrows indicate directions of increase (decrease) of I_h. (**b**) Scatter plots of theta and gamma peak frequencies and power (normalized).
doi:10.1371/journal.pone.0076285.g010

modulations of theta and gamma oscillations could be utilized by functional mechanisms that are postulated to utilize linkages between theta and gamma to provide encodings such as phase precession in place cells [49], cross-frequency coupling (CFC) [35,50–52], and gamma on theta phase for memory [20]. Indeed, our model demonstrated that shifting oscillatory modulations were effective in setting the CFC level, with increases evident at high theta PYR I_h levels (Fig. 12e). We therefore predict the presence of distinct neurotransmitter receptor types in PYR and BAS cells which would allow I_h to be tuned independently, and therefore support flexible shifting of the CFC level.

Our model demonstrated that increased PYR I_h would increase PYR excitability, augment PYR → BAS feedforward activation via a PING mechanism, and thereby shift gamma activation to an earlier phase within the theta cycle. In the context of neural coding, the timing of pyramidal cell firing within a theta cycle has been hypothesized to allow the most relevant neurons for a particular stimulus to fire at earlier phases and then inhibit firing of other ensembles [53]. Our model suggests how modulation of I_h could enhance this contrast sensitivity by enhancing this initial activation. This is also consistent with recent experimental work that demonstrates the contribution of I_h currents to hippocampal pyramidal neuron synchronization [54], which could cause downstream neurons to fire earlier, thereby modulating timing of gamma spikes.

Intracellular signalling can be used to modulate the degree to which I_h is regulated. This has been demonstrated experimentally in the heart [14,55], and similar mechanisms may take place in neurons via neuromodulatory control [11]. This mechanism has been demonstrated in computer models of prefrontal cortex neurons [17]. In this process, the neuron is initially activated via feedforward excitatory inputs. With sufficiently strong activation, calcium is admitted. Subsequently, calcium binds to protein kinases (*e.g.*, cAMP) which bind to HCN and increase I_h conductance, leading to increased excitability. Our model shows that in the neuronal network context, this process leads to frequency tuning, increased CFC, and earlier generation of

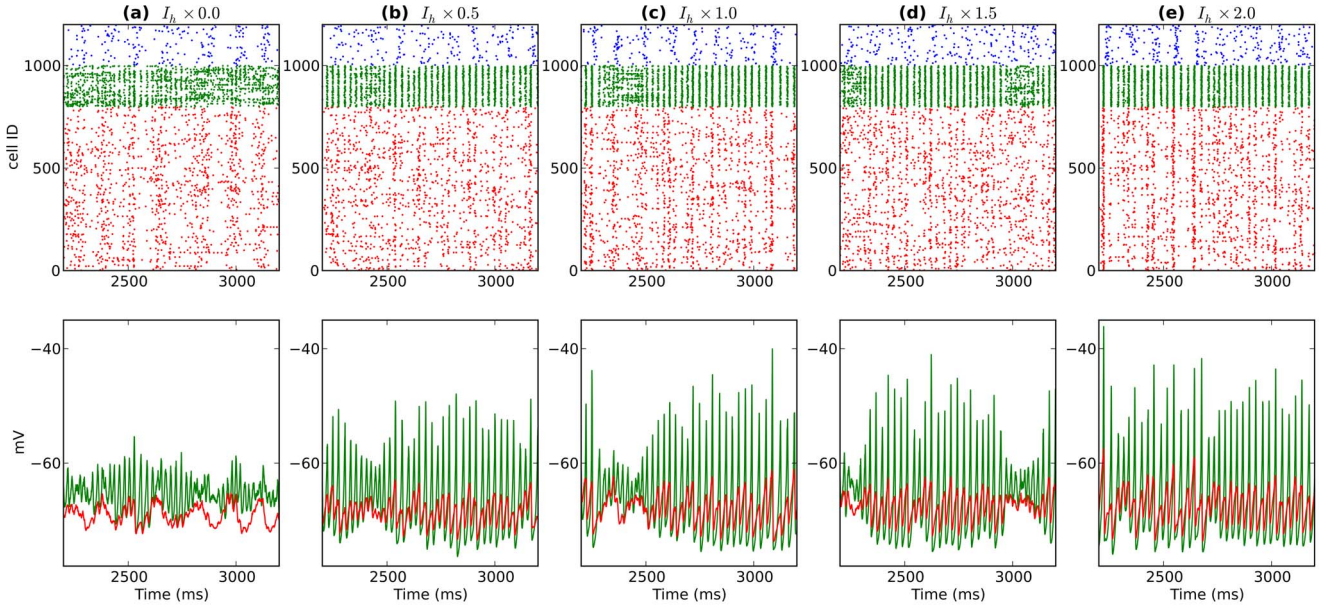

Figure 11. Activity from a single network after modulating PYR and BAS I_h levels (PYR and BAS I_h increases left to right). Top shows spike rasters (PYR:red; BAS:green; OLM:blue). Bottom displays average somatic voltage from PYR (red; $n=800$) and BAS (green; $n=200$) cells.
doi:10.1371/journal.pone.0076285.g011

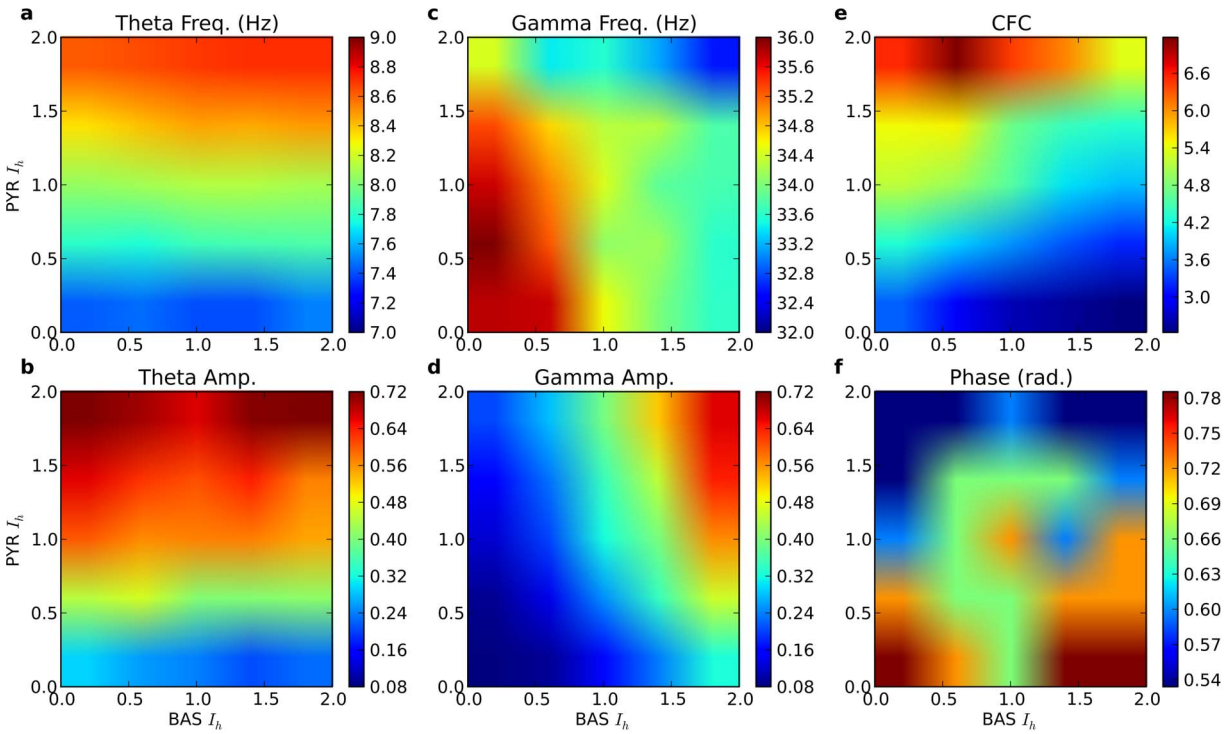

Figure 12. Amplitudes and coupling of oscillations with variation of I_h density in BAS and PYR cells (x- and y-axes, respectively). (**a**) Theta frequency and (**b**) amplitude are controlled by PYR I_h, while (**c**) Gamma frequency and (**d**) amplitude are largely controlled by BAS I_h. (**e**) Cross-frequency coupling (gamma amplitude modulation by theta phase) is greatest when theta is strong (high PYR I_h) with gamma relatively weak. Units are scaled up by 1e3 for readability. (**f**) Gamma amplitude peaks in the region between $\frac{\pi}{6}$ (0.5) and $\frac{\pi}{4}$ (0.8) radians in a complex pattern. (a,b,c,d: average of 900 8s simulations; e,f: average of 25 900 s simulations).
doi:10.1371/journal.pone.0076285.g012

gamma spikes by the activated cells. Due to long time constants of protein kinase binding with HCN, the effects of this initial activation could be used to prime a circuit's response to subsequent inputs.

Our current model remains limited by lack of explicit second messenger modeling and lack of detailed information about differences between HCN isoforms. In particular, cAMP, the second messenger which acts on I_h, also has effects on K^+ [56] or leak [6,57] channels, which would also tend to change cell and network dynamics. Our HCN isoform modeling also remains limited, since we only included electrophysiological, and not second messenger, differences. Inclusion of second messenger signaling pathways will be of greatest value once further details are available concerning differences in second messenger responsitivity between the two major isoforms studied here. Further detail might also consider differences in phosphorylation states which provide further modulation of these channels [58].

Acknowledgments

The authors would like to thank Antonio Carlos Roque da Silva Filho (University of Sao Paulo) for organizing *Latin American School of Computational Neuroscience IV* (University of Sao Paulo, Ribeirao Preto, Brazil), where this research was begun; Herman Moreno (SUNY Downstate) for discussions; Michael Hines and Ted Carnevale (Yale) for NEURON support; Tom Morse (Yale) for ModelDB support; Larry Eberle and Amy Delman (SUNY Downstate) for Neurosim lab support; the anonymous reviewers for their helpful comments.

Author Contributions

Conceived and designed the experiments: SAN WWL. Performed the experiments: SAN MH TM YS. Analyzed the data: SAN MH TM YS MTL WWL. Contributed reagents/materials/analysis tools: MTL. Wrote the paper: SAN WWL.

References

1. Accili E, Proenza C, Baruscotti M, DiFrancesco D (2002) From funny current to HCN channels: 20 years of excitation. Physiology 17: 32–37.
2. Chen S, Wang J, Siegelbaum S (2001) Properties of hyperpolarization-activated pacemaker current defined by coassembly of HCN1 and HCN2 subunits and basal modulation by cyclic nucleotide. Journal Gen Physiol 117: 491–504.
3. Santoro B, Baram T (2003) The multiple personalities of h-channels. Trends Neurosci 26: 550–554.
4. Zemankovics R, Káli S, Paulsen O, Freund T, Hájos N (2010) Differences in subthreshold resonance of hippocampal pyramidal cells and interneurons: the role of h-current and passive membrane characteristics. J Physiol 588: 2109–2132.
5. Dyhrfjeld-Johnsen J, Morgan R, Soltesz I (2009) Double trouble? potential for hyperexcitability following both channelopathic up-and downregulation of Ih in epilepsy. Front Neurosci 3: 25.
6. Poolos N, Migliore M, Johnston D (2002) Pharmacological upregulation of h-channels reduces the excitability of pyramidal neuron dendrites. Nat Neurosci 5: 767–774.
7. Bender R, Brewster A, Santoro B, Ludwig A, Hofmann F, et al. (2001) Differential and age-dependent expression of hyperpolarization-activated, cyclic nucleotide-gated cation channel isoforms 1-4 suggests evolving roles in the developing rat hippocampus. Neuroscience 106: 689–698.
8. Dyhrfjeld-Johnsen J, Morgan R, Földy C, Soltesz I (2008) Upregulated H-Current in hyperexcitable CA1 dendrites after febrile seizures. Front Cell Neurosci 2.
9. Aponte Y, Lien C, Reisinger E, Jonas P (2006) Hyperpolarization-activated cation channels in fast-spiking interneurons of rat hippocampus. J Physiol 574: 229–243.
10. Carr D, Andrews G, Glen W, Lavin A (2007) α2-noradrenergic receptors activation enhances excitability and synaptic integration in rat prefrontal cortex pyramidal neurons via inhibition of hcn currents. J Physiol 584: 437–450.
11. Heys J, Hasselmo M (2012) Neuromodulation of Ih in layer II medial entorhinal cortex stellate cells: a voltage-clamp study. J Neurosci 32: 9066–9072.
12. Tsuno Y, Schultheiss N, Hasselmo M (2013) In vivo cholinergic modulation of the cellular properties of medial entorhinal cortex neurons. J Physiol 591: 2611–2627.
13. Wang M, Ramos B, Paspalas C, Shu Y, Simen A, et al. (2007) α2a-adrenoceptors strengthen working memory networks by inhibiting cAMP-HCN channel signaling in prefrontal cortex. Cell 129: 397–410.
14. Hagiwara N, Irisawa H (1989) Modulation by intracellular ca2+ of the hyperpolarization-activated inward current in rabbit single sino-atrial node cells. J Physiol 409: 121–141.
15. Buzsáki G, Wang X (2012) Mechanisms of gamma oscillations. Annu Rev Neurosci 35: 203–225.
16. Freund T, Buzsáki G (1996) Interneurons of the hippocampus. Hippocampus 6: 347–470.
17. Winograd M, Destexhe A, Sanchez-Vives M (2008) Hyperpolarization-activated graded persistent activity in the prefrontal cortex. Proc Natl Acad Sci USA 105: 7298–7303.
18. Neymotin S, Lazarewicz M, Sherif M, Contreras D, Finkel L, et al. (2011) Ketamine disrupts theta modulation of gamma in a computer model of hippocampus. J Neurosci 31: 11733–11743.
19. Lakatos P, Karmos G, Mehta A, Ulbert I, Schroeder C (2008) Entrainment of neuronal oscillations as a mechanism of attentional selection. Science 320: 110–113.
20. Lisman J, Idiart M (1995) Storage of 7 ± 2 short-term memories in oscillatory subcycles. Science 267: 10.
21. Tort A, Komorowski R, Manns J, Kopell N, Eichenbaum H (2009) Theta-gamma coupling increases during the learning of item-context associations. Proc Nat Acad Sci 106: 20942–20947.
22. Carnevale N, Hines M (2006) The NEURON Book. New York: Cambridge University Press.
23. Hines M, Davison A, Muller E (2009) NEURON and Python. Front Neuroinform 3: 1.
24. Lytton W (2006) Neural query system: data-mining from within the NEURON simulator. Neuroinformatics 4: 163–176.
25. Tort A, Rotstein H, Dugladze T, Gloveli T, Kopell N (2007) On the formation of gamma-coherent cell assemblies by oriens lacunosum-moleculare interneurons in the hippocampus. Proc Natl Acad Sci U S A 104: 13490–13495.
26. Wang X, Buzsaki G (1996) Gamma oscillation by synaptic inhibition in a hippocampal interneuronal network model. J Neurosci 16: 6402–6413.
27. Wang X (2002) Pacemaker neurons for the theta rhythm and their synchronization in the septohippocampal reciprocal loop. J Neurophysiol 87: 889–900.
28. McCormick D, Huguenard J (1992) A model of the electrophysiological properties of thalamocortical relay neurons. J Neurophysiol 68: 1384–1400.
29. Migliore M, Messineo L, Ferrante M (2004) Dendritic Ih selectively blocks temporal summation of unsynchronized distal inputs in CA1 pyramidal neurons. J Comput Neurosci 16: 5–13.
30. Stacey W, Lazarewicz M, Litt B (2009) Synaptic noise and physiological coupling generate high-frequency oscillations in a hippocampal computational model. J Neurophysiol 102: 2342–2357.
31. White J, Banks M, Pearce R, Kopell N (2000) Networks of interneurons with fast and slow γ–aminobutyric acid type A (GABAA) kinetics provide substrate for mixed gamma-theta rhythm. Proc Nat Acad Sci 97: 8128–8133.
32. Jahr C, Stevens C (1990) Voltage dependence of NMDA-activated macroscopic conductances predicted by single-channel kinetics. J Neurosci 10: 3178–3182.
33. Destexhe A, Rudolph M, Paré D (2003) The high-conductance state of neocortical neurons in vivo. Nat Rev Neurosci 4: 739–751.
34. Oppenheim A, Schafer R, Buck J (1999) Discrete-time signal processing. Prentice Hall, Upper Saddle River, N.J., 2nd ed.
35. Tort A, Kramer M, Thorn C, Gibson D, Kubota Y, et al. (2008) Dynamic cross-frequency couplings of local field potential oscillations in rat striatum and hippocampus during performance of a t-maze task. Proc Nat Acad Sci 105: 20517–20522.
36. Kramer M, Tort A, Kopell N (2008) Sharp edge artifacts and spurious coupling in EEG frequency comodulation measures. J Neurosci Methods 170: 352–357.
37. Neymotin S, Uhlrich D, Manning K, Lytton W (2008) Data mining of time-domain features from neural extracellular field data. Studies in Computational Intelligence 151: 119–140.
38. Börgers C, Kopell N (2003) Synchronization in networks of excitatory and inhibitory neurons with sparse, random connectivity. Neural Comput 15: 509–538.
39. Lytton W, Sejnowski T (1991) Simulations of cortical pyramidal neurons synchronized by inhibitory interneurons. J Neurophysiol 66: 1059–1079.
40. Marcelin B, Chauvière L, Becker A, Migliore M, Esclapez M, et al. (2009) H channel-dependent deficit of theta oscillation resonance and phase shift in temporal lobe epilepsy. Neurobiol Dis 33: 436–447.
41. Wahl-Schott C, Biel M (2009) HCN channels: structure, cellular regulation and physiological function. Cel Mol Life Sci 66: 470–494.
42. Zong X, Krause S, Chen C, Krüger J, Gruner C, et al. (2012) Regulation of hyperpolarization-activated cyclic nucleotide-gated (HCN) channel activity by cCMP. J Biol Chem 287: 26506–26512.

43. Poolos NP, Bullis JB, Roth MK (2006) Modulation of h-channels in hippocampal pyramidal neurons by p38 mitogen-activated protein kinase. J Neurosci 26: 7995–8003.
44. Belluscio M, Mizuseki K, Schmidt R, Kempter R, Buzsaki G (2012) Cross-frequency phase-phase coupling between theta and gamma oscillations in the hippocampus. J Neurosci 32: 423–435.
45. Canolty R, Knight R (2010) The functional role of cross-frequency coupling. Trends Cogn Sci 14.
46. Schroeder C, Lakatos P (2009) The gamma oscillation: master or slave. Brain Topogr 22: 24–26.
47. Wang J, Chen S, Nolan M, Siegelbaum S (2002) Activity-dependent regulation of HCN pacemaker channels by cyclic AMP: signaling through dynamic allosteric coupling. Neuron 36: 451–461.
48. Newman E, Gillet S, Climer J, Hasselmo M (2012) Effects of cholinergic modulation on interactions of entorhinal cortex and hippocampus as measured by theta modulation of high and low gamma in the rat. Society for Neuroscience Abstracts 42.
49. O'Keefe J, Recce M (1993) Phase relationship between hippocampal place units and the EEG theta rhythm. Hippocampus 3: 317–330.
50. Caixeta F, Cornélio A, Scheffer-Teixeira R, Ribeiro S, Tort A (2013) Ketamine alters oscillatory coupling in the hippocampus. Sci Rep 3: 2348.
51. Canolty R, Edwards E, Dalal S, Soltani M, Nagarajan S, et al. (2006) High gamma power is phase-locked to theta oscillations in human neocortex. Science 313: 1626–1628.
52. Lee H, Dvorak D, Kao H, Duffy Á, Scharfman H, et al. (2012) Early cognitive experience prevents adult deficits in a neurodevelopmental schizophrenia model. Neuron 75: 714–724.
53. de Almeida L, Idiart M, Lisman J (2009) A second function of gamma frequency oscillations: an E%-max winner-take-all mechanism selects which cells fire. J Neurosci 29: 7497–7503.
54. Hilscher M, Leão K, Leão R (2013) Synchronization through nonreciprocal connections in a hybrid hippocampus microcircuit. Front Neural Circuits 7: 120.
55. El Khoury N, Mathieu S, Marger L, Ross J, El Gebeily G, et al. (2013) Upregulation of the hyperpolarizationactivated current increases pacemaker activity of the sinoatrial node and heart rate during pregnancy in mice. Circulation 127: 2009–2020.
56. Arnsten A, Paspalas C, Gamo N, Yang Y, Wang M (2010) Dynamic Network Connectivity: a new form of neuroplasticity. Trends Cogn Sci 14: 365–375.
57. Migliore M, Migliore R (2012) Know your current Ih: Interaction with a shunting current explains the puzzling effects of its pharmacological or pathological modulations. PloS One 7: e36867.
58. Robinson R, Siegelbaum S (2003) Hyperpolarization-activated cation currents: from molecules to physiological function. Annu Rev Physiol 65: 453–480.